JPE 19-4-15

https://doi.org/10.6113/JPE.2019.19.4.1000
ISSN(Print): 1598-2092 / ISSN(Online): 2093-4718

Transient-Performance-Oriented Discrete-Time Design of Resonant Controller for Three-Phase Grid-Connected Converters

Zhanfeng Song†, Yun Yu*, Yaqi Wang*, and Xiaohui Ma*

†,*School of Electrical and Information Engineering, Tianjin University, Tianjin, China

Abstract

The use of internal-model-based linear controller, such as resonant controller, is a well-established technique for the current control of grid-connected systems. Attractive properties for resonant controllers include their two-sequence tracking ability, the simple control structure, and the reduced computational burden. However, in the case of continuous-designed resonant controller, the transient performance is inevitably degraded at a low switching frequency. Moreover, available design methods for resonant controller is not able to realize the direct design of transient performances, and the anticipated transient performance is mainly achieved through trial and error. To address these problems, the zero-order-hold (ZOH) characteristic and inherent time delay in digital control systems are considered comprehensively in the design, and a corresponding hold-equivalent discrete model of the grid-connected converter is then established. The relationship between the placement of closed-loop poles and the corresponding transient performance is comprehensively investigated to realize the direct mapping relationship between the control gain and the transient response time. For the benefit of automatic tuning and real-time adaption, analytical expressions for controller gains are derived in detail using the required transient response time and system parameters. Simulation and experimental results demonstrate the validity of the proposed method.

Key words: Discrete-time design, Grid-connected converters, Resonant controller, Transient performance

I. INTRODUCTION

Grid-connected voltage-source converters (VSCs) have gained a large popularity in recent years due to the growing use of renewable energy and the wide implementation of distributed power generation systems (DPGSs) [1]. In these power generation systems, VSCs serve as the power conversion equipment which transforms the power to meet the requirements for grid interconnection [2], [3]. Filters are normally installed between the converter and utility network to attenuate high frequency harmonics generated by the switching actions of power electronic devices [4]-[6]. Considering the enhancement of power quality, the performance of grid-connected converter should be designed to meet the stricter requirements [7]. Generally, a fast dynamic response without oscillations and a low current THD are anticipated.

The control structure of VSCs is usually based on the cascaded control scheme, where the inner control loop is normally used to regulate currents [8], [9]. In this case, the performance of the inner loop has a significant impacts on the overall control performance [10]. Among the various current controllers, including both linear and nonlinear controllers, resonant controllers are widely adopted due to their simple control structure and reduced computational burden [9], [11]-[13]. For example, resonant controllers can regulate both positive-sequence and negative-sequence currents at the same time without any modifications [14], [15], which is a good property for unbalanced operation conditions [16], [17]. In this manner, resonant controllers are suitable for the control of DPGSs, since the two-sequence-tracking ability benefits the ride-through capability of DPGSs [18], [19]. Another attractive feature is the elimination of multi-frequency harmonics, which can be realized directly by using multiple resonant controllers [20]-[23], since each resonant controller only produces an infinite gain for the corresponding

Manuscript received Jan. 2, 2019; accepted Mar. 21, 2019
Recommended for publication by Associate Editor Hao Ma.
†Corresponding Author: zfsong@tju.edu.cn
Tel: +86-022-27890065, Tianjin University
*School of Electrical and Information Eng., Tianjin University, China

frequency signal. This straightforward implementation simplifies the control structure for power quality improvement [20], [21]. Generally, zero steady-state error can be achieved when resonant controllers are implemented, and the transient response and the desired transient response time are focuses of resonant control [24], [25]. For most applications, it is expected that controllers be designed with an accurate dynamic response [26], [27].

An available method for the design of resonant controllers is based on a continuous-time analysis, where the model of the plant is normally established in the continuous-time domain using transfer functions [21], [28], [29]. In this manner, a frequency-response analysis is normally applied, and the bandwidth is then adopted as a major factor for the evaluation of close-loop dynamics. Nevertheless, in real applications, the designed controllers are normally applied in digital control systems [30]. Electrical quantities like the currents and voltages are sampled for control, and pulse-width modulation (PWM) is applied for the realization of the control voltage. In addition, an inherent time delay always exists in the digital control system. Thus, the discrete characteristics of this type of sampled-data system should be taken into account comprehensively during modeling [15], [31], [32]. Based on an accurate discrete-time model, the stability can be really ensured, and the desired system dynamics can be realized correspondingly, especially when the system is designed with high dynamics and a relatively low switching frequency [15], [25].

In terms of the current controller design, another important aspect is the transient response which has been extensively investigated in many studies. For example, in [33], an approach utilizing the sliding-mode control is proposed for the current loop of grid-forming inverters, and the proposed algorithm can produce a fast and robust tracking performance even under parameter variations. Due to its satisfactory transient response, a sliding-mode-control-based current loop is also applied in [34] for the primary control of an isolated ac microgrid. It is worth noting that, for the design of conventional linear controller, such as proportional integral (PI) controller, a well-established approach is to obtain the desired time-domain specifications [27]. Following this manner, the transient response time of the dc signal tracking can be directly determined. However, for resonant control in ac systems, the similar performance is difficult to achieve. One design method that focuses on the transient performance is presented in [26], where the optimal transient is obtained by assessing the influence of the proportional and resonant gain on the closed-loop poles and zeros. However, the direct mapping relationship between the control gains and the transient response time is not available. Additionally, in [27], the anticipated transient performance is attained using continuous-time design, where the performance is inevitably deteriorated in the case of a low switching frequency.

Controller tuning is another important task that has a significant influence on the performance of the entire control system. For example, when offline tuning methods are applied, the controller parameters are invariant, and the control performance can be degraded due to the variations of the system parameters [35]. For the benefits of realizing satisfactory control performance, accurate automatic tuning methods are preferable [24], [32]. To ensure stable operations and to improve the dynamic response, an automatic tuning algorithm has been proposed for power converters with cascaded control loops in [36]. It is worth noting that, the automatic tuning also makes the implementation of real-time adaption realizable, where the system parameters can be measured or estimated for the tuning of the controller gains. For DPGSs, the power plants may be installed in remote areas, and the impedance of these plants may not always be constant. Thus, a simple and straightforward controller tuning algorithm can benefit the controllability improvement in these cases.

This paper presents a transient-performance-oriented resonant control for grid-connected VSCs. The contributions of this paper can be summarized as follow. The accurate hold-equivalent discrete model of the grid-connected converter is established, where the ZOH characteristic of the PWM and the inherent time delay are simultaneously taken into account. In this manner, improved stability of the resonant control can be obtained, especially in the case of a reduced switching frequency. Moreover, the direct mapping relationship between the control gain and the transient response time of resonant control is presented with given time-domain specifications. Following this direct mapping relationship, the closed-loop poles and zeros are configured to achieve a desired transient performance. In addition, to realize the automatic tuning of the proposed resonant control, analytical expressions for the controller gains are derived directly using the desired transient performance and system parameters.

This paper is organized as follows. In Section II, a generalized plant is analyzed, and a hold-equivalent model in the discrete-time domain is then presented. In Section III, the design of the controller is presented in detail, and the selection of closed-loop poles for a desired transient performance is given. The analytical expressions are derived in Section IV. Experimental results are presented and analyzed in Section V. The conclusions are drawn in Section VI.

II. System Model

In this paper, the boldfaced letters are used to donate matrices or complex vectors, and the complex vector quantities are expressed in stationary $\alpha\beta$ coordinates (e.g., current vector $\boldsymbol{i}_c = i_{c\alpha} + \mathrm{j}i_{c\beta}$). In the following, the continuous-time model of the generalized circuit is firstly

presented. Then the corresponding hold-equivalent discrete-time model is established for the controller design.

The dynamic of the generalized circuit in the continuous-time domain can be expressed using state differential and output equations as:

$$\begin{aligned}\dot{\boldsymbol{x}}(t) &= -\frac{R_{\mathrm{f}}}{L_{\mathrm{f}}}\boldsymbol{x}(t)+\frac{1}{L_{\mathrm{f}}}\boldsymbol{u}_{\mathrm{c}}(t)-\frac{1}{L_{\mathrm{f}}}\boldsymbol{u}_{\mathrm{g}}(t)\\ \boldsymbol{i}_{\mathrm{c}}(t) &= \boldsymbol{x}(t)\end{aligned} \tag{1}$$

where $\boldsymbol{u}_{\mathrm{c}}(t)$ represents the output voltage of the converter, $\boldsymbol{u}_{\mathrm{g}}(t)$ stands for the voltage at the point of common coupling, and $\boldsymbol{i}_{\mathrm{c}}(t)$ stands for the output current of the convert. In addition, the symmetrical three-phase impedance of the grid interconnection is marked by resistance R_{f} and inductance L_{f}, respectively.

In order to directly design resonant controllers in the discrete-time domain, the continuous-time model of the system should be transformed into the discrete-time model using an appropriate approach, which can accurately reveal the characteristics of the digital control system. Typically, the sampling instances are synchronized with PWM. As a result, the impact of electromagnet interference on the sampling process can be released, and the sampled current ripple can be avoided. When the PWM is single updated, the sampling frequency is equal to the switching frequency. In the case of double-update PWM, the sampling frequency is twice of the switching frequency. Additionally, the sampled current and output voltage are kept constant between two sampling instants. Considering the ZOH characteristics of the sampling and PWM, the corresponding hold-equivalent discrete-time model is given as:

$$\begin{aligned}\boldsymbol{x}(k+1) &= \phi\boldsymbol{x}(k)+\tau_{\mathrm{c}}\boldsymbol{u}_{\mathrm{c}}(k)+\tau_{\mathrm{g}}\boldsymbol{u}_{\mathrm{g}}(k)\\ \boldsymbol{i}_{\mathrm{c}}(k) &= \boldsymbol{x}(k)\end{aligned} \tag{2}$$

where the system matrices can be formulated as (3), and T_{S} is the sampling period.

$$\begin{aligned}&\phi = e^{-R_{\mathrm{f}}T_{\mathrm{s}}/L_{\mathrm{f}}},\ \tau_{\mathrm{c}} = \frac{1}{L_{\mathrm{f}}}\int_0^{T_{\mathrm{s}}} e^{-R_{\mathrm{f}}\eta/L_{\mathrm{f}}}d\eta,\\ &\tau_{\mathrm{g}} = -\frac{1}{L_{\mathrm{f}}}\int_0^{T_{\mathrm{s}}} e^{-R_{\mathrm{f}}\eta/L_{\mathrm{f}}}d\eta\end{aligned} \tag{3}$$

With the adopted synchronous sampling mode, an inherent one-sample-period delay always exists. In other words, the sampled current at the present sampling instant k is used to generate the control voltage to be applied at the next instant k +1. This computational delay can be formulated by $\boldsymbol{u}_{\mathrm{c}}(k+1)=\boldsymbol{u}_{\mathrm{c,ref}}(k)$. In order to include the computational delay in the discrete-time model, the model augmentation is applied. The corresponding augmented plant model is given as:

$$\begin{aligned}&\underbrace{\begin{bmatrix}\boldsymbol{x}(k+1)\\ \boldsymbol{u}_{\mathrm{c}}(k+1)\end{bmatrix}}_{\mathbf{x}_{\mathrm{d}}(k+1)}=\underbrace{\begin{bmatrix}\phi & \tau_{\mathrm{c}}\\ 0 & 0\end{bmatrix}}_{\boldsymbol{\Phi}_{\mathrm{d}}}\underbrace{\begin{bmatrix}\boldsymbol{x}(k)\\ \boldsymbol{u}_{\mathrm{c}}(k)\end{bmatrix}}_{\mathbf{x}_{\mathrm{d}}(k)}+\underbrace{\begin{bmatrix}0\\ 1\end{bmatrix}}_{\boldsymbol{\Gamma}_{\mathrm{cd}}}\boldsymbol{u}_{\mathrm{c,ref}}(k)+\underbrace{\begin{bmatrix}\tau_{\mathrm{g}}\\ 0\end{bmatrix}}_{\boldsymbol{\Gamma}_{\mathrm{gd}}}\boldsymbol{u}_{\mathrm{g}}(k)\\ &\boldsymbol{i}_{\mathrm{c}}(k)=\underbrace{\begin{bmatrix}1 & 0\end{bmatrix}}_{\mathbf{H}_{\mathrm{d}}}\underbrace{\begin{bmatrix}\boldsymbol{x}(k)\\ \boldsymbol{u}_{\mathrm{c}}(k)\end{bmatrix}}_{\mathbf{x}_{\mathrm{d}}(k)}\end{aligned} \tag{4}$$

where $\mathbf{x}_{\mathrm{d}}$ is the new state variable. $\boldsymbol{\Phi}_{\mathrm{d}}$, $\boldsymbol{\Gamma}_{\mathrm{cd}}$, $\boldsymbol{\Gamma}_{\mathrm{gd}}$ and $\mathbf{H}_{\mathrm{d}}$ denote the system matrices.

III. Transient-Performance-Oriented Discrete-Time Design of a Resonant Controller

A. Discrete-Time Design of Resonant Controller

According to the internal model principle, for zero steady-state error, the model of external disturbances should be embedded in the controller. For the resonant control implemented in the stationary coordinates, the sinusoidal signals can be regarded as an external disturbance, which can be modeled as:

$$\ddot{d}(t) = -\omega_0^2 d(t) \tag{5}$$

where $d(t)$ represents the sinusoidal signals, and ω_0 is the frequency of the sinusoidal signals. In general, the state-space formulation corresponding to (5) can be written as:

$$\begin{bmatrix}\dot{\boldsymbol{x}}_{\mathrm{I1}}(t)\\ \dot{\boldsymbol{x}}_{\mathrm{I2}}(t)\end{bmatrix}=\begin{bmatrix}0 & \omega_0\\ -\omega_0 & 0\end{bmatrix}\begin{bmatrix}\boldsymbol{x}_{\mathrm{I1}}(t)\\ \boldsymbol{x}_{\mathrm{I2}}(t)\end{bmatrix} \tag{6}$$

where $\boldsymbol{x}_{\mathrm{I1}}(t)$ and $\boldsymbol{x}_{\mathrm{I2}}(t)$ are two integral states corresponding to the sinusoidal signals.

In order to avoid discretization errors, the resonant poles in the discrete-time domain should have an accurate mapping relationship with those in the continuous-time domain. In this way, the discrete-time poles are set to $e^{\pm \mathrm{j}\omega_0 T_{\mathrm{s}}}$, and the discrete form of (6) can be written as:

$$\begin{bmatrix}\boldsymbol{x}_{\mathrm{I1}}(k+1)\\ \boldsymbol{x}_{\mathrm{I2}}(k+1)\end{bmatrix}=\begin{bmatrix}0 & 1\\ -1 & 2\cos(\omega_0)\end{bmatrix}\begin{bmatrix}\boldsymbol{x}_{\mathrm{I1}}(k)\\ \boldsymbol{x}_{\mathrm{I2}}(k)\end{bmatrix} \tag{7}$$

For pole placement, two integral states $\boldsymbol{x}_{\mathrm{I1}}(k)$ and $\boldsymbol{x}_{\mathrm{I2}}(k)$ should be included in the model of the plant [30]. The discrete-time model (4) is then augmented with the internal model (7), resulting in:

$$\begin{aligned}&\underbrace{\begin{bmatrix}\mathbf{x}_{\mathrm{d}}(k+1)\\ \mathbf{x}_{\mathrm{I1}}(k+1)\\ \mathbf{x}_{\mathrm{I2}}(k+1)\end{bmatrix}}_{\mathbf{x}_{\mathrm{a}}(k+1)}=\underbrace{\begin{bmatrix}\boldsymbol{\Phi}_{\mathrm{d}} & \mathbf{0} & \mathbf{0}\\ \mathbf{0} & 0 & 1\\ \mathbf{H}_{\mathrm{d}} & -1 & T\end{bmatrix}}_{\boldsymbol{\Phi}_{\mathrm{a}}}\underbrace{\begin{bmatrix}\mathbf{x}_{\mathrm{d}}(k)\\ \mathbf{x}_{\mathrm{I1}}(k)\\ \mathbf{x}_{\mathrm{I2}}(k)\end{bmatrix}}_{\mathbf{x}_{\mathrm{a}}(k)}+\underbrace{\begin{bmatrix}\boldsymbol{\Gamma}_{\mathrm{cd}}\\ 0\\ 0\end{bmatrix}}_{\boldsymbol{\Gamma}_{\mathrm{ca}}}\boldsymbol{u}_{\mathrm{c,ref}}(k)\\ &\qquad-\underbrace{\begin{bmatrix}\mathbf{0}\\ 0\\ 1\end{bmatrix}}_{\boldsymbol{\Gamma}_{\mathrm{ra}}}\boldsymbol{i}_{\mathrm{c,ref}}(k)+\underbrace{\begin{bmatrix}\boldsymbol{\Gamma}_{\mathrm{gd}}\\ 0\\ 0\end{bmatrix}}_{\boldsymbol{\Gamma}_{\mathrm{ga}}}\boldsymbol{u}_{\mathrm{g}}(k)\end{aligned} \tag{8}$$

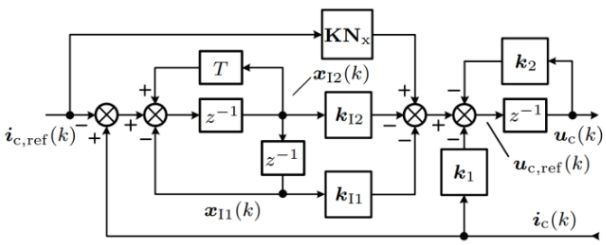

Fig. 1. Block diagram of the proposed resonant control with full state feedback.

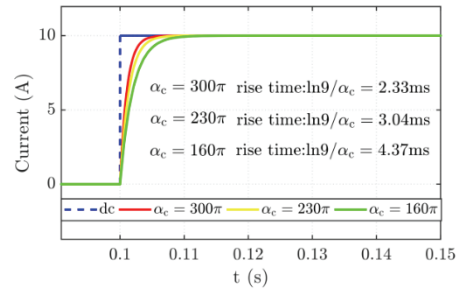

Fig. 2. Transient Response of dc signal tracking.

where $\mathbf{x}_a$ is the new state variable; $\mathbf{\Phi}_a$, $\mathbf{\Gamma}_{ca}$, $\mathbf{\Gamma}_{ra}$ and $\mathbf{\Gamma}_{ga}$ are the new system matrices; and T is used to represent the coefficient $2\cos(\omega_0 T_s)$.

As shown in Fig. 1, in the proposed resonant controller, a reference feedforward path and a current feedback path are applied as the well-established state-space controller. Moreover, in order to realize more degrees of freedom for the resonant control, two integral states are both used in the controller, and a state corresponding to the previous control voltage is used as well. Correspondingly, the control law can be written as:

$$\boldsymbol{u}_{c,ref}(k) = -\underbrace{\begin{bmatrix}\mathbf{K} & \mathbf{K}_I\end{bmatrix}}_{\mathbf{K}_a}\underbrace{\begin{bmatrix}\mathbf{x}_d(k)\\ \boldsymbol{x}_I(k)\end{bmatrix}}_{\mathbf{x}_a(k)} + \mathbf{KN}_x\boldsymbol{i}_{c,ref}(k) \tag{9}$$

where $\mathbf{K}_a = [\mathbf{K},\ \mathbf{K}_I]$ is the state-feedback gain after augmentation; $\mathbf{K} = [\boldsymbol{k}_1,\ \boldsymbol{k}_2]$ is the gain of the original states; $\mathbf{K}_I = [\boldsymbol{k}_{I1},\ \boldsymbol{k}_{I2}]$ is the gain of the two integral states; and $\boldsymbol{x}_I(k) = [\boldsymbol{x}_{I1}(k),\ \boldsymbol{x}_{I2}(k)]$ stands for the integral states. Reference-feedforward is applied as well, and the corresponding gain is $\mathbf{KN}_x$. From (8) and (9), the dynamic of the closed-loop system is given as:

$$\begin{aligned}\mathbf{x}_a(k+1) &= (\mathbf{\Phi}_a - \mathbf{\Gamma}_{ca}\mathbf{K}_a)\mathbf{x}_a(k)\\ &\quad + (\mathbf{KN}_x\mathbf{\Gamma}_{ca} + \mathbf{\Gamma}_{ra})\boldsymbol{i}_{c,ref}(k) + \mathbf{\Gamma}_{ga}\boldsymbol{u}_g(k)\\ \boldsymbol{i}_c(k) &= \mathbf{H}_a\mathbf{x}_a(k).\end{aligned} \tag{10}$$

where $\mathbf{H}_a = [\mathbf{H}_d,\ 0,\ 0]$ is the output matrix. To mitigate the negative influences of grid voltage, the measured grid voltage is directly added into the controller output.

B. Transient-Performance-Oriented Design

There is a close connection between the transient tracking performance of the closed-loop control system and the controller properties. For the benefit of the controller design, the transient response time of the control loop should be directly designed by selecting the controller parameters. For example, when the control loop is designed for the tracking of dc signals, the reference of the control loop is:

$$i^*(t) = Au(t) \tag{11}$$

where A stands for the amplitude of the reference step.

It is well established that when the corresponding closed-loop system is configured to be a first-order plant, the tracking error between the actual plant output and the reference can be then formulated as:

$$e(t) = Ae^{-\alpha_c t} \tag{12}$$

where α_c is the bandwidth of the first-order plant.

In this manner, for the tracking of dc signals, different transient response time can be realized when the parameter α_c is set to different values. As shown in Fig. 2, by selecting α_c, different transient response time can be obtained correspondingly. In a similar manner, for ac reference tracking, it is anticipated that the transient response can be designed by properly selecting the controller parameters.

For the regulation of ac signals, the sinusoidal reference of the control loop can be written as:

$$i^*(t) = A\sin(\omega_0 t)u(t) \tag{13}$$

In order to make the transient response time of the afore-mentioned dc signal tracking and that of the ac signal tracking approximately the same, the expected tracking error in ac systems can be formulated as:

$$e(t) = Ae^{-\alpha_c t}\sin(\omega_0 t) \tag{14}$$

To realize the tracking error as (14), the closed-loop poles of (10) need to be configured corresponding to different values of α_c, which is similar to the direct design of the transient response time in the dc system. It should be noted that, as can be derived from (8), there are four open-loop poles that need to be placed. Specifically, the pole originating from the delay locates at $z = 0$, and another pole introduced by the original plant locates at $e^{-R_f T_s / L_f}$. Moreover, the internal model (7) introduces two extra open-loop poles at $e^{\pm j\omega_0 T_s}$.

With the control law as (9) applied, the aforementioned four open-loop poles can be arbitrarily placed in the closed-loop systems. Assuming the closed-loop poles are placed at the desired locations, the characteristic polynomial is given as:

$$\boldsymbol{a}(z) = (z - \boldsymbol{\alpha}_0)(z - \boldsymbol{\alpha}_1)(z - \boldsymbol{\alpha}_2)(z - \boldsymbol{\alpha}_3) \tag{15}$$

where $\boldsymbol{\alpha}_0$, $\boldsymbol{\alpha}_1$, $\boldsymbol{\alpha}_2$ and $\boldsymbol{\alpha}_3$ are the desired closed-loop poles. Since the pole originating from the delay is already optimal, it remains in the same location. In order to achieve the desired transient process as (14), two complex poles introduced by the internal model of the sinusoidal signals are chosen to be the dominant poles. Additionally, the real pole

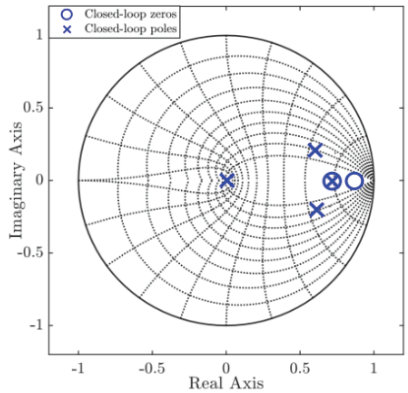

Fig. 3. Explanation of the designed pole placement.

introduced by the original plant remains in the same place, and it can be canceled by the zero. In this way, the desired closed-loop poles can be expressed as:

$$\boldsymbol{\alpha}_0 = 0,\ \boldsymbol{\alpha}_1 = e^{-R_f T_s / L_f},\ \boldsymbol{\alpha}_{2,3} = e^{T_s(-\alpha_c \pm j\omega_0)} \tag{16}$$

In addition to the closed-loop poles, two zeros originating from the reference feedforward need to be placed properly. One of the zeros is set to $\boldsymbol{\alpha}_1$, and another zero is set to $z_1 = e^{(-\alpha_c T_s/2)}$, as it is indicated in Fig. 3. Once the pole placement is determined, the controller gains can be automatically tuned using analytical expressions.

In order to demonstrate that the controller proposed in this paper can realize the direct design of the transient response time, simulation validation is applied. According to the above-mentioned poles and zeros, the closed-loop transfer function of the designed system in the discrete-time domain can be directly written as:

$$G(z) = \frac{z - z_1}{z(z - \boldsymbol{\alpha}_2)(z - \boldsymbol{\alpha}_3)} \tag{17}$$

To verify the tracking performance of the designed controller, two different ac references are tested in simulation, and the corresponding expressions are given as:

$$I^*_{\sin}(z) = \frac{z\sin(\omega_0 T_s)}{z^2 - 2z\cos(\omega_0 T_s) + 1} \tag{18}$$

$$I^*_{\cos}(z) = \frac{z[z - \cos(\omega_0 T_s)]}{z^2 - 2z\cos(\omega_0 T_s) + 1} \tag{19}$$

Using the closed-loop transfer function and the ac references, the response of the ac signal tracking can be easily obtained, as it is shown in Fig. 4 and Fig. 5. To clearly illustrate the designable transient response time, simulation results of the dc system mentioned previously are also included in Fig. 4 and Fig. 5. It can be seen that the dc signal can be regarded as the envelope of the ac signal in both steady state and transient process. In this manner, the transient response time of ac reference tracking in resonant control can be directly designed, which is similar to the well-established design in dc systems.

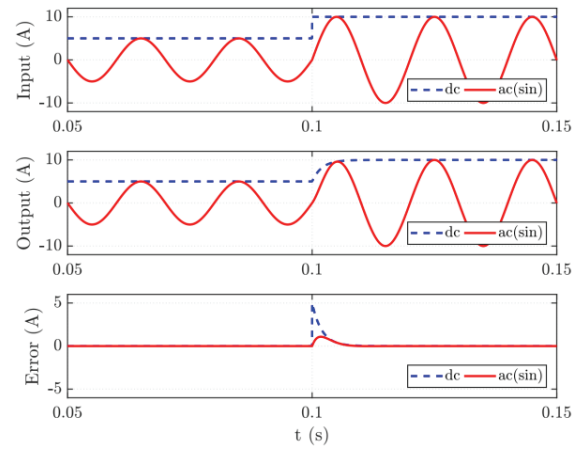

Fig. 4. Response of the designed current loop when input is (18).

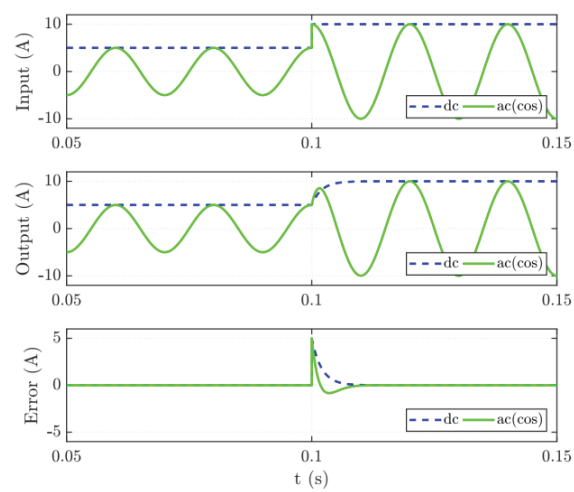

Fig. 5. Response of the designed current loop when input is (19).

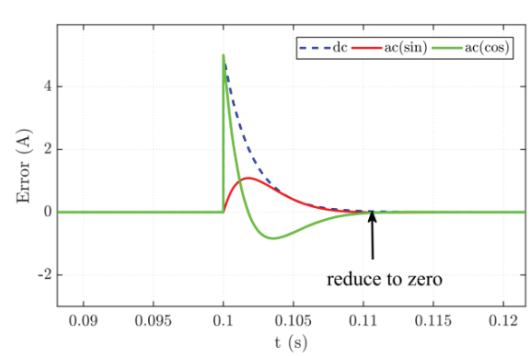

Fig. 6. Tracking errors during the transient process.

To further illustrate the anticipated performance, the tracking errors of both dc and ac signals in Fig. 4 and Fig. 5 are placed in a single figure, as it is shown in Fig. 6. It can be seen that the tracking errors of the designed system are eliminated within a certain time, and that the transient response times of both ac and the dc systems are the same. Therefore, in the design of resonant control, different values of α_c can be selected according to the desired transient response time. Then different poles and zeros are configured correspondingly to obtain the desired transient response time.

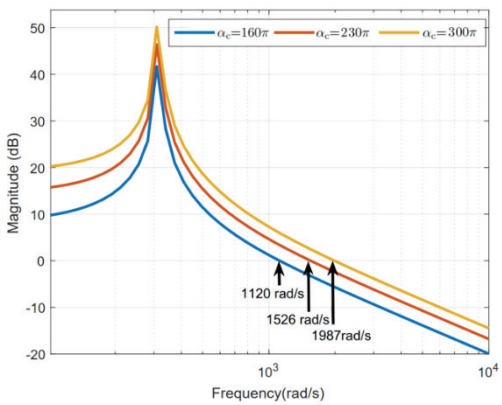

Fig. 7. Bode plots of the open-loop transfer function.

In addition, in order to analyze the relationship between the parameter α_c and the crossover frequency of the resonant control loop, the open-loop transfer function of the designed system can be written as:

$$G_{ol}(z) = \frac{z - z_1}{z(z-\alpha_2)(z-\alpha_3)-(z-z_1)} \tag{20}$$

The frequency response of (20), with the parameter α_c set to different values, is shown in Fig. 7. It can be seen that when the parameter α_c grows linearly, the crossover frequency of the resonant control loop is not linearly linked to α_c. In addition, the corresponding relationship between the crossover frequency and transient response time cannot be directly established. Thus, compared with the proposed design method, methods based on the direct selection of crossover frequency cannot be used to achieve the previously discussed designable transient response time.

IV. Analytical Gain Expressions

A. State-Feedback Gain

The desired characteristic polynomial (15) can be written as:

$$\boldsymbol{a}(z) = z^4 + \boldsymbol{a}_3 z^3 + \boldsymbol{a}_2 z^2 + \boldsymbol{a}_1 z + \boldsymbol{a}_0 \tag{21}$$

The coefficients of the polynomial are then expressed as functions of the closed-loop poles.

$$\begin{aligned} &\boldsymbol{a}_0 = 0,\ \boldsymbol{a}_1 = -\boldsymbol{\alpha}_1\boldsymbol{\alpha}_2\boldsymbol{\alpha}_3 \\ &\boldsymbol{a}_2 = \boldsymbol{\alpha}_1\boldsymbol{\alpha}_2 + \boldsymbol{\alpha}_1\boldsymbol{\alpha}_3 + \boldsymbol{\alpha}_2\boldsymbol{\alpha}_3 \\ &\boldsymbol{a}_3 = -\boldsymbol{\alpha}_1 - \boldsymbol{\alpha}_2 - \boldsymbol{\alpha}_3 \end{aligned} \tag{22}$$

The characteristic polynomial of the closed-loop system (10) is:

$$\begin{aligned} \boldsymbol{a}(z) &= \det(z\mathbf{I} - \boldsymbol{\Phi}_a + \boldsymbol{\Gamma}_{ca}\mathbf{K}_a) \\ &= z^4 + (\boldsymbol{k}_2 - \phi - T)z^3 + [\tau_c\boldsymbol{k}_1 - (\phi+T)\boldsymbol{k}_2 + T\phi \\ &\quad +1]z^2 + [-T\tau_c\boldsymbol{k}_1 + (T\phi+1)\boldsymbol{k}_2 + \tau_c\boldsymbol{k}_{12} - \phi]z \\ &\quad +\tau_c(\boldsymbol{k}_1 + \boldsymbol{k}_{11}) - \phi\boldsymbol{k}_2 \end{aligned} \tag{23}$$

From (21) and (23), the coefficients of the polynomial are expressed as the functions of the system parameters and state-feedback gains. Taking (22) into account, the relationships among the state-feedback gains, system parameters, and closed-loop poles are then established as:

$$\underbrace{\begin{bmatrix} \boldsymbol{m}_{11} & \boldsymbol{m}_{12} & \boldsymbol{m}_{13} & \boldsymbol{m}_{14} \\ \boldsymbol{m}_{21} & \boldsymbol{m}_{22} & \boldsymbol{m}_{23} & \boldsymbol{m}_{24} \\ \boldsymbol{m}_{31} & \boldsymbol{m}_{32} & \boldsymbol{m}_{33} & \boldsymbol{m}_{34} \\ \boldsymbol{m}_{41} & \boldsymbol{m}_{42} & \boldsymbol{m}_{43} & \boldsymbol{m}_{44} \end{bmatrix}}_{\mathbf{M}} \underbrace{\begin{bmatrix} \boldsymbol{k}_1 \\ \boldsymbol{k}_2 \\ \boldsymbol{k}_{11} \\ \boldsymbol{k}_{12} \end{bmatrix}}_{\mathbf{K}_a^{\mathrm{T}}} = \underbrace{\begin{bmatrix} \boldsymbol{w}_1 \\ \boldsymbol{w}_2 \\ \boldsymbol{w}_3 \\ \boldsymbol{w}_4 \end{bmatrix}}_{\mathbf{W}} \tag{24}$$

where the elements of the matrix **M** are:

$$\begin{aligned} &\boldsymbol{m}_{12} = -\phi,\ \boldsymbol{m}_{21} = -T\tau_c \\ &\boldsymbol{m}_{22} = T\phi + 1,\ \boldsymbol{m}_{32} = -\phi - T \\ &\boldsymbol{m}_{11} = \boldsymbol{m}_{13} = \boldsymbol{m}_{24} = \boldsymbol{m}_{31} = \tau_c \\ &\boldsymbol{m}_{14} = \boldsymbol{m}_{23} = \boldsymbol{m}_{33} = \boldsymbol{m}_{34} = \boldsymbol{m}_{41} = \boldsymbol{m}_{43} = \boldsymbol{m}_{44} = 0. \end{aligned} \tag{25}$$

In additon, the elements of the matrix **W** are:

$$\begin{aligned} &\boldsymbol{w}_1 = \boldsymbol{a}_0,\ \boldsymbol{w}_2 = \boldsymbol{a}_1 + \phi, \\ &\boldsymbol{w}_3 = \boldsymbol{a}_2 - T\phi - 1,\ \boldsymbol{w}_4 = \boldsymbol{a}_3 + \phi + T. \end{aligned} \tag{26}$$

The state-feedback gains can be obtained by solving $\mathbf{K}_a^{\mathrm{T}} = \mathbf{M}^{-1}\mathbf{W}$. However, it is difficult to accomplish this task in real-time applications. In order to realize real-time adaption, the matrix **M** in (24) is rewritten as:

$$\mathbf{M} = \underbrace{\begin{bmatrix} 1 & 0 & 0 & 0 \\ \boldsymbol{l}_{21} & 1 & 0 & 0 \\ \boldsymbol{l}_{31} & \boldsymbol{l}_{32} & 1 & 0 \\ \boldsymbol{l}_{41} & \boldsymbol{l}_{42} & \boldsymbol{l}_{43} & 1 \end{bmatrix}}_{\mathbf{L}} \underbrace{\begin{bmatrix} \boldsymbol{u}_{11} & \boldsymbol{u}_{12} & \boldsymbol{u}_{13} & \boldsymbol{u}_{14} \\ 0 & \boldsymbol{u}_{22} & \boldsymbol{u}_{23} & \boldsymbol{u}_{24} \\ 0 & 0 & \boldsymbol{u}_{33} & \boldsymbol{u}_{34} \\ 0 & 0 & 0 & \boldsymbol{u}_{44} \end{bmatrix}}_{\mathbf{U}} \tag{27}$$

where the elements of the lower diagonal matrix **L** are:

$$\begin{aligned} &\boldsymbol{l}_{21} = \boldsymbol{m}_{21}/\boldsymbol{m}_{11},\ \boldsymbol{l}_{31} = \boldsymbol{m}_{31}/\boldsymbol{m}_{11},\ \boldsymbol{l}_{41} = \boldsymbol{m}_{41}/\boldsymbol{m}_{11} \\ &\boldsymbol{l}_{32} = (\boldsymbol{m}_{32} - \boldsymbol{l}_{31}\boldsymbol{u}_{12})/\boldsymbol{u}_{22},\ \boldsymbol{l}_{42} = (\boldsymbol{m}_{42} - \boldsymbol{l}_{41}\boldsymbol{u}_{12})/\boldsymbol{u}_{22} \\ &\boldsymbol{l}_{43} = (\boldsymbol{m}_{42} - \boldsymbol{l}_{41}\boldsymbol{u}_{13} - \boldsymbol{l}_{42}\boldsymbol{u}_{23})/\boldsymbol{u}_{33} \end{aligned} \tag{28}$$

and the elements of the upper diagonal matrix **U** are:

$$\begin{aligned} &\boldsymbol{u}_{11} = \boldsymbol{m}_{11},\ \boldsymbol{u}_{12} = \boldsymbol{m}_{12},\ \boldsymbol{u}_{13} = \boldsymbol{m}_{13},\ \boldsymbol{u}_{14} = \boldsymbol{m}_{14} \\ &\boldsymbol{u}_{22} = \boldsymbol{m}_{22} - \boldsymbol{l}_{21}\boldsymbol{u}_{12},\ \boldsymbol{u}_{23} = \boldsymbol{m}_{23} - \boldsymbol{l}_{21}\boldsymbol{u}_{13} \\ &\boldsymbol{u}_{24} = \boldsymbol{m}_{24} - \boldsymbol{l}_{21}\boldsymbol{u}_{14},\ \boldsymbol{u}_{33} = \boldsymbol{m}_{33} - \boldsymbol{l}_{31}\boldsymbol{u}_{13} - \boldsymbol{l}_{32}\boldsymbol{u}_{23} \\ &\boldsymbol{u}_{34} = \boldsymbol{m}_{34} - \boldsymbol{l}_{31}\boldsymbol{u}_{14} - \boldsymbol{l}_{32}\boldsymbol{u}_{24} \\ &\boldsymbol{u}_{44} = \boldsymbol{m}_{44} - \boldsymbol{l}_{41}\boldsymbol{u}_{14} - \boldsymbol{l}_{42}\boldsymbol{u}_{24} - \boldsymbol{l}_{43}\boldsymbol{u}_{34} \end{aligned} \tag{29}$$

The auxiliary matrix $\mathbf{C} = [\boldsymbol{c}_1, \boldsymbol{c}_2, \boldsymbol{c}_3, \boldsymbol{c}_4]^{\mathrm{T}}$ is introduced. Assuming $\mathbf{C} = \mathbf{L}^{-1}\mathbf{W}$, the elements of the auxiliary matrix are expressed as:

$$\begin{aligned} &\boldsymbol{c}_1 = \boldsymbol{w}_1,\ \boldsymbol{c}_2 = \boldsymbol{w}_2 - \boldsymbol{l}_{21}\boldsymbol{c}_1 \\ &\boldsymbol{c}_3 = \boldsymbol{w}_3 - \boldsymbol{l}_{31}\boldsymbol{c}_1 - \boldsymbol{l}_{32}\boldsymbol{c}_2 \\ &\boldsymbol{c}_4 = \boldsymbol{w}_4 - \boldsymbol{l}_{41}\boldsymbol{c}_1 - \boldsymbol{l}_{42}\boldsymbol{c}_2 - \boldsymbol{l}_{43}\boldsymbol{c}_3 \end{aligned} \tag{30}$$

The analytical expressions for the controller gains are expressed as:

$$\begin{aligned} &\boldsymbol{k}_{12} = \boldsymbol{c}_4 / \boldsymbol{u}_{44}, \ \boldsymbol{k}_{11} = (\boldsymbol{c}_3 - \boldsymbol{u}_{34}\boldsymbol{k}_{12}) / \boldsymbol{u}_{33} \\ &\boldsymbol{k}_2 = (\boldsymbol{c}_2 - \boldsymbol{u}_{23}\boldsymbol{k}_{11} - \boldsymbol{u}_{24}\boldsymbol{k}_{12}) / \boldsymbol{u}_{22} \\ &\boldsymbol{k}_1 = (\boldsymbol{c}_1 - \boldsymbol{u}_{12}\boldsymbol{k}_2 - \boldsymbol{u}_{13}\boldsymbol{k}_{11} - \boldsymbol{u}_{14}\boldsymbol{k}_{12}) / \boldsymbol{u}_{11} \end{aligned} \tag{31}$$

B. Reference-Feedforward Gain

The numerator polynomial obtained from the closed-loop model (10) is given as:

$$\boldsymbol{b}(z) = \tau_c[\mathbf{KN}_x z^2 - (\mathbf{KN}_x T - \boldsymbol{k}_{12})z + \mathbf{KN}_x + \boldsymbol{k}_{11}] \tag{32}$$

As mentioned previously, one of the closed-loop zeros is used to cancel the pole $\boldsymbol{\alpha}_1$. Then the corresponding reference-feedforward gain is given as:

$$\mathbf{KN}_x = -(\boldsymbol{k}_{11} + \boldsymbol{k}_{12}\boldsymbol{\alpha}_1) / (\boldsymbol{\alpha}_1^2 - T\boldsymbol{\alpha}_1 + 1) \tag{33}$$

V. Simulation and Experimental Results

The performance of the proposed resonant control is experimentally verified with the experimental setup shown in Fig. 8. In the experiments, a 7.5-kW Danfoss VSC is used, and the control signals for VSC are received by the interface board installed on the converter. The control algorithms are implemented in a DSP TMS320F28379D, and the PWM implemented in the control system is set to double-update mode. For the safe operation of the switching devices, dead time is added in the PWM. The parameters of the entire experimental setup are listed in the Table I, and the structure of the current control system in the experiment is shown as Fig. 9.

In order to evaluate the transient response of the proposed controller, a step in the amplitude of the current references is generated, and the corresponding experimental results are shown in Fig. 10. As can be observed, the tracking error in β axis is negligible, and it is primarily introduced by the dead time effect. In this way, the tracking error is mainly introduced in the α axis. When the parameter α_c is set to 160π, the tracking error in the α axis is eliminated in approximately 4.33ms. It should be noted that, according to the analysis, the error elimination time is 4.37ms (ln9/160π). Thus, the actual transient response time of the designed resonant control can approximately match that of the analysis. In Fig. 11, the error drops to zero in approximately 3.00ms when α_c is set to 230π, which can still correspond to the analysis (ln9/230π = 3.04ms). In Fig. 12, the transient process is approximately 2.32ms, and it also fits the analysis, which is 2.33ms (ln9/300π = 2.33ms). These results verify the direct mapping relationship between the control gain and the transient response time. In particular, the transient processes contain no oscillation, and the smooth transient processes improve the stability of the grid-connected system. In grid-connected systems, the total harmonic distortion (THD) of the injected currents should be lower than 5%. In order to

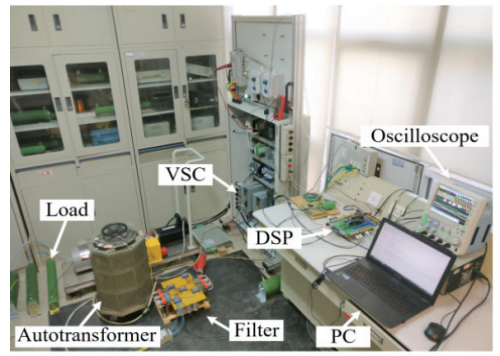

Fig. 8. Photo of the experimental setup.

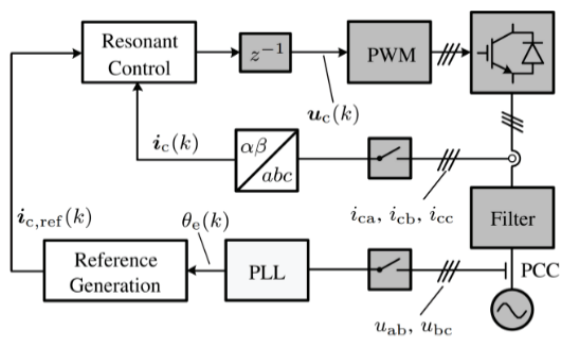

Fig. 9. Current control system.

confirm the THD of the grid current, a harmonic analysis is applied, and the results are presented in Fig. 13. As can be observed, with the parameters of the proposed controller set to different values, the THD is approximately the same. Additionally, in these cases, the THD of the grid current is always below 5%, which can satisfy the standards for grid interconnection.

Additionally, to confirm the improved stable behavior introduced by the discrete-time design, the sampling frequency and the switching frequency of the converter are reduced, and the corresponding transient response is tested. For comparison, the continuous-time design method is also tested in the experiments. In the continuous-time design, the same pole placement is applied, and the designed controllers are discretized using Tustin with the prewarping method for minimization of the discretization error. In this manner, the difference between the continuous-time design and the discrete-time design is the model used for pole placement.

As shown in Fig. 14(a) and 15(a), the transient response time of both the continuous-time-designed controller and the discrete-time-designed controller are approximately the same in the case of f_s = 5kHz. For a further comparison, the switching frequency of the converter is reduced to 4kHz. The effectiveness of the continuous-time design method is degraded, since oscillations start to occur in the current of α axis, as shown in Fig. 15(b). However, under the same conditions, the discrete-time design method can produce approximately the same transient response time as the analysis, and the transient process is smooth without

TABLE I
SYSTEM PARAMETERS

Parameter	Symbol	Value	Parameter	Symbol	Value
Rated power	P_N	7.5 kW	L filter inductance	L_f	6.6 mH
Dead time	T_d	4 μs	Sampling frequency	f_{samp}	6/12 kHz
DC link load	L_d	175 Ω	Switching frequency	f_s	3/6 kHz
L filter resistance	R_f	0.03 Ω	Controller parameter	α_c	160π/300π rad/s

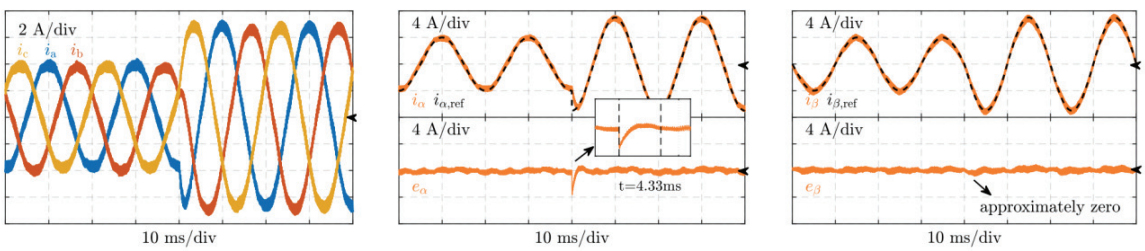

(a) (b) (c)

Fig. 10. Dynamic response with $\alpha_c = 160\pi$ and $f_s = 6$kHz. (a) Three-phase currents. (b) Current and error in α axis. (c) Current and error in β axis.

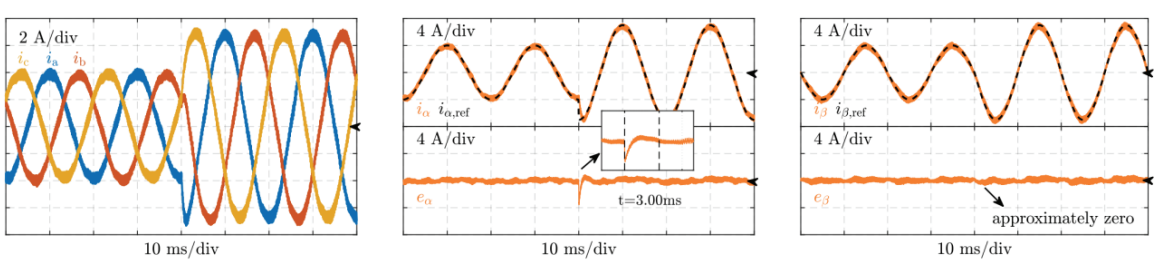

(a) (b) (c)

Fig. 11. Dynamic response with $\alpha_c = 230\pi$ and $f_s = 6$kHz. (a) Three-phase currents. (b) Current and error in α axis. (c) Current and error in β axis.

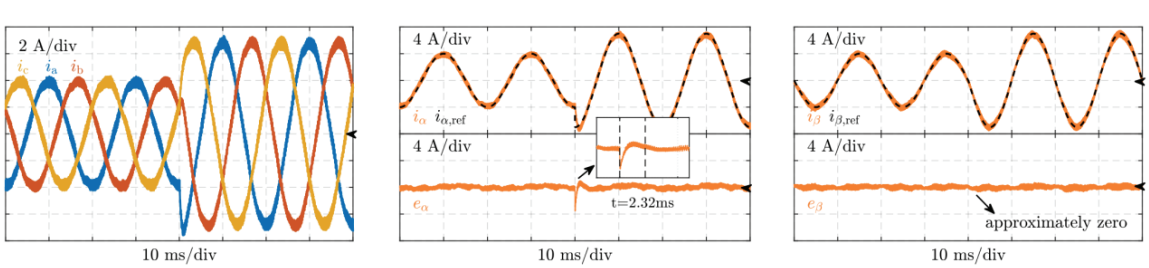

(a) (b) (c)

Fig. 12. Dynamic response with $\alpha_c = 300\pi$ and $f_s = 6$kHz. (a) Three-phase currents. (b) Current and error in α axis. (c) Current and error in β axis.

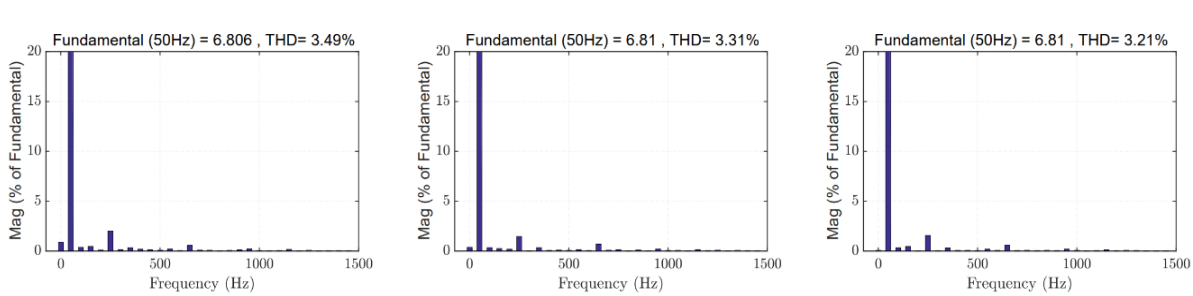

(a) (b) (c)

Fig. 13. THD of the grid side currents. (a) $\alpha_c = 160\pi$ and $f_s = 6$kHz. (b) $\alpha_c = 230\pi$ and $f_s = 6$kHz. (c) $\alpha_c = 300\pi$ and $f_s = 6$kHz.

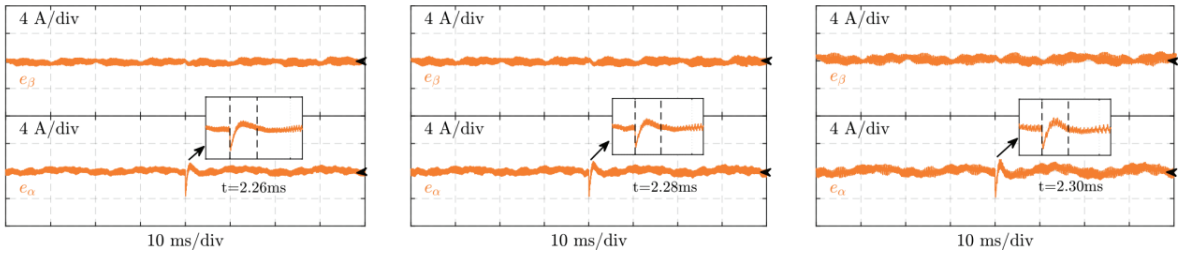

Fig. 14. Dynamic response of the discrete-time design with $\alpha_c = 300\pi$ and different f_s. (a) f_s = 5kHz. (b) f_s = 4kHz. (c) f_s = 3kHz.

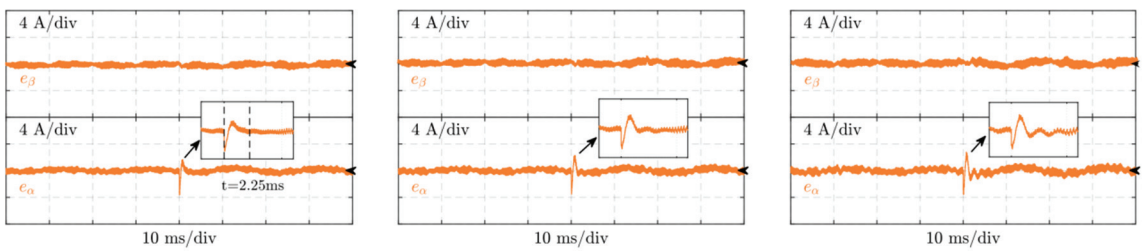

Fig. 15. Dynamic response of the continuous-time design with $\alpha_c = 300\pi$ and different f_s. (a) f_s = 5kHz. (b) f_s = 4kHz. (c) f_s = 3kHz.

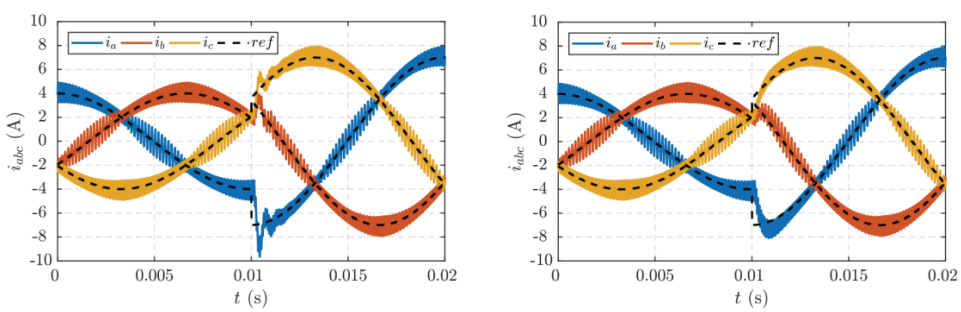

Fig. 16. Simulation comparison with the conventional method. (a) The conventional linear controller. (b) The proposed transient-performance-oriented resonant controller.

oscillations, as can observed in Fig. 14(b). When the switching frequency is further reduced to 3.5kHz, the continuous-time design method fails to guarantee its performance during the transient process. In addition, obvious oscillations can be observed, as indicated in Fig. 15(c). As a comparison, even when the switching frequency is set to 3kHz, the discrete-time design method can still produce a relatively good performance during the transient process. It worth noting that the error- elimination time is approximately 2.30ms, which still corresponds to the analysis, as indicated in Fig. 14(c).

To produce a comparison between the conventional linear controller and the proposed controller, the well-established method presented in [37] is applied, and the corresponding simulation results are presented in Fig. 16. As can be observed in Fig. 16(a), when the conventional method is applied, undesired oscillations occur in the transient process. However, under the same test conditions, the transient response is fast without obvious oscillations when the proposed controller is adopted, as shown in Fig. 16(b).

VI. Conclusion

In this paper, a transient-performance-oriented resonant controller is proposed for the current control of grid- connected converters. Specifically, for the direct discrete-time design, an accurate discrete-time hold-equivalent model is established with the ZOH characteristic and the digital delay simultaneously taken into account. According to the direct mapping relationship between the control gain and the transient response time, the poles and zeros are precisely configured to achieve the desired transient performance. In order to implement the controller automatic tuning straight-forwardly, the analytical expressions for the controller gains are given as functions of desired transient response time and system parameters. When compared with the corresponding continuous-time design, the proposed method can guarantee the transient performance even under a low switching frequency. Additionally, all of the properties of resonant controllers, such as the two-sequence tracking capability, the simple control structure, and the reduced computational burden are perfectly

retained. For validation, a number of simulations and experiments are carried out, and the corresponding results confirm that the proposed transient-performance-oriented design method can realize the direct design of the transient response time.

ACKNOWLEDGMENT

This paper is supported by the National Natural Science Foundation of China (Grant No.51877150, No.51477113).

REFERENCES

[1] B. K. Bose, "Global energy scenario and impact of power electronics in 21st century," *IEEE Trans. Ind. Electron*., Vol. 60, No. 7, pp. 2638-2651, Jul. 2013.

[2] F. Blaabjerg, Z. Chen, and S. B. Kjaer, "Power electronics as efficient interface in dispersed power generation systems," *IEEE Trans. Power Electron*., Vol. 19, No. 5, pp. 1184-1194, Sep. 2004.

[3] J. M. Carrasco, L. G. Franquelo, J. T. Bialasiewicz, E. Galvan, R. C. P. Guisado, M. A. M. Prats, J. I. Leon, and N. Moreno-Alfonso, "Power-electronic systems for the grid integration of renewable energy sources: A survey," *IEEE Trans. Ind. Electron*., Vol. 53, No. 4, pp. 1002-1016, Jun. 2006.

[4] R. N. Beres, X. F. Wang, M. Liserre, F. Blaabjerg, and C. L. Bak, "A review of passive power filters for three-phase grid-connected voltage-source converters," *IEEE J. Emerg. Sel. Topics Power Electron*., Vol. 4, No. 1, pp. 54-69, Mar. 2016.

[5] M. Liserre, F. Blaabjerg, and S. Hansen, "Design and control of an LCL-filter-based three-phase active rectifier," *IEEE Trans. Ind. Appl*., Vol. 41, No. 5, pp. 1281-1291, Sep. 2005.

[6] Y. W. Li, "Control and resonance damping of voltage-source and current-source converters with LC filters," *IEEE Trans. Ind. Electron*., Vol. 56, No. 5, pp. 1511-1521, May. 2009.

[7] M. H. Bollen, *Understanding Power Quality Problems: Voltage Sags and Interruptions*, Wiley, 2001.

[8] J. W. He and Y. W. Li, "Generalized closed-loop control schemes with embedded virtual impedances for voltage source converters with LC or LCL filters," *IEEE Trans. Power Electron*., Vol. 27, No. 4, pp. 1850-1861, Apr. 2012.

[9] F. Blaabjerg, R. Teodorescu, M. Liserre, and A. V. Timbus, "Overview of control and grid synchronization for distributed power generation systems," *IEEE Trans. Ind. Electron*., Vol. 53, No. 5, pp. 1398-1409, Oct. 2006.

[10] M. P. Kazmierkowski and L. Malesani, "Current control techniques for three-phase voltage-source PWM converters: a survey," *IEEE Trans. Ind. Electron*., Vol. 45, No. 5, pp. 691-703, Oct. 1998.

[11] A. Timbus, M. Liserre, R. Teodorescu, P. Rodriguez, and F. Blaabjerg, "Evaluation of current controllers for distributed power generation systems," *IEEE Trans. Power Electron*., Vol. 24, No. 3, pp. 654-664, Mar. 2009.

[12] D. N. Zmood and D. G. Holmes, "Stationary frame current regulation of PWM inverters with zero steady-state error," *IEEE Trans. Power Electron*., Vol. 18, No. 3, pp. 814-822, May. 2003.

[13] Y. Sato, T. Ishizuka, K. Nezu, and T. Kataoka, "A new control strategy for voltage-type PWM rectifiers to realize zero steady-state control error in input current," *IEEE Trans. Ind. Appl*., Vol. 34, No. 3, pp. 480-486, May. 1998.

[14] D. N. Zmood, D. G. Holmes, and G. H. Bode, "Frequency-domain analysis of three-phase linear current regulators," *IEEE Trans. Ind. Appl*., Vol. 37, No. 2, pp. 601-610, Mar. 2001.

[15] D. Perez-Estevez, J. Doval-Gandoy, A. G. Yepes, and O. Lopez, "Positive- and negative-sequence current controller with direct discrete-time pole placement for grid-tied converters with LCL filter," *IEEE Trans. Power Electron*., Vol. 32, No. 9, pp. 7207-7221, Sep. 2017.

[16] J. B. Hu and Y. K. He, "Modeling and control of grid-connected voltage-sourced converters under generalized unbalanced operation conditions," *IEE Trans. Energy Convers*., Vol. 23, No. 3, pp. 903-913, Sep. 2008.

[17] H. Song and K. Nam, "Dual current control scheme for PWM converter under unbalanced input voltage conditions," *IEEE Trans. Ind. Electron*., Vol. 46, No. 5, pp. 953-959, Oct. 1999.

[18] X. H. Wang, D. Sun, and Z. Q. Zhu, "Resonant-based backstepping direct power control strategy for DFIG under both balanced and un-balanced grid conditions," *IEEE Trans. Ind. Appl.*, Vol. 53, No. 5, pp. 4821-4830, Sep. 2017.

[19] J. B. Hu and Y. K. He, "Reinforced control and operation of DFIG-based wind-power-generation system under unbalanced grid voltage conditions," *IEE Trans. Energy Convers*., Vol. 24, No. 4, pp. 905-915, Dec. 2009.

[20] X. M. Yuan, W. Merk, H. Stemmler, and J. Allmeling, "Stationary-frame generalized integrators for current control of active power filters with zero steady-state error for current harmonics of concern under unbalanced and distorted operating conditions," *IEEE Trans. Ind. Appl*., Vol. 38, No. 2, pp. 523-532, Mar. 2002.

[21] M. Castilla, J. Miret, J. Matas, L. G. de Vicuna, and J. M. Guerrero, "Control design guidelines for single-phase grid-connected photovoltaic inverters with damped resonant harmonic compensators," *IEEE Trans. Ind. Electron*., Vol. 56, No. 11, pp. 4492-4501, Nov. 2009.

[22] C. L. Xia, B. N. Ji, and Y. Yan, "Smooth speed control for low-speed high-torque permanent-magnet synchronous motor using proportional-integral-resonant controller," *IEEE Trans. Ind. Electron*., Vol. 62, No. 4, pp. 2123-2134, Apr. 2015.

[23] C. Peng, J. J. Sun, X. D. Song, and J. C. Fang, "Frequency-varying current harmonics for active magnetic bearing via multiple resonant controllers," *IEEE Trans. Ind. Electron*., Vol. 64, No. 1, pp. 517-526, Jan. 2017.

[24] D. Perez-Estevez, J. Doval-Gandoy, A. G. Yepes, O. Lopez, and F.Baneira, "Enhanced resonant current controller for grid-connected converters with LCL filter," *IEEE Trans. Power Electron*., Vol. 33, No. 5, pp. 3765-3778, May. 2017.

[25] C. A. Busada, S. G. Jorge, and J. A. Solsona, "Resonant current controller with enhanced transient response for grid-tied inverters," *IEEE Trans. Ind. Electron*., Vol. 65, No. 4, pp. 2935-2944, Apr. 2018.

[26] A. Vidal, F. D. Freijedo, A. G. Yepes, P. Fernandez-Comesana, J. Malvar, O.Lopez, and J. Doval-Gandoy, "Assessment and optimization of the transient response of proportional-resonant current controllers for dis-tributed power generation systems," *IEEE Trans. Ind. Electron*., Vol. 60, No. 4, pp. 1367-1383, Apr. 2013.

[27] A. Kuperman, "Proportional-resonant current controllers design based on desired transient performance," *IEEE Trans. Power Electron*., Vol. 30, No. 10, pp. 5341-5345, Oct. 2015.
[28] D. G. Holmes, T. A. Lipo, B. P. McGrath, and W. Y. Kong, "Optimized design of stationary frame three phase ac current regulators," *IEEE Trans. Power Electron*., Vol. 24, No. 11, pp. 2417-2426, Nov. 2009.
[29] G. Q. Shen, X. C. Zhu, J. Zhang, and D. H. Xu, "A new feedback method for PR current control of LCL-filter-based grid-connected inverter," *IEEE Trans. Ind. Electron*., Vol. 57, No. 6, pp. 2033-2041, Jun. 2010.
[30] G. F. Franklin, J. D. Powell, and M. L. Workman, *Digital Control of Dynamic Systems*, Menlo Park, CA, USA: Addison-Wesley, 1997.
[31] A. G. Yepes, F. D. Freijedo, O. Lopez, and J. Doval-Gandoy, "Analysis and design of resonant current controllers for voltage-source converters by means of nyquist diagrams and sensitivity function," *IEEE Trans. Ind. Electron*., Vol. 58, No. 11, pp. 5231-5250, Nov. 2011.
[32] J. Kukkola, M. Hinkkanen, and K. Zenger, "Observer-based state-space current controller for a grid converter equipped with an LCL filter: Analytical method for direct discrete-time design," *IEEE Trans. Ind. Appl*., Vol. 51, No. 5, pp. 4079-4090, Sep. 2015.
[33] Z. W. Li, C. Z. Zang, P. Zeng, H. B. Yu, S. H. Li, and B. Jing, "Control of a grid-forming inverter based on sliding mode and mixed H2=H1 control," *IEEE Trans. Ind. Electron*., Vol. 64, No. 5, pp. 3862-3872, May. 2017.
[34] Z. W. Li, C. Z. Zang, P. Zeng, H. B. Yu, and S. H. Li, "Fully distributed hierarchical control of parallel grid-supporting inverters in islanded AC microgrids," *IEEE Trans. Ind. Informat*., Vol. 14, No. 2, pp. 679-690, Feb. 2018.
[35] W. L. Chen and J. S. Lin, "One-dimensional optimization for proportional-resonant controller design against the change in source impedance and solar irradiation in PV systems," *IEEE Trans. Ind. Electron*., Vol. 61, No. 4, pp. 1845-1854, Apr. 2014.
[36] S. D'Arco, J. A. Suul, and O. B. Fosso, "Automatic tuning of cascaded controllers for power converters using eigenvalue parametric sensitivi-ties," *IEEE Trans. Ind. Appl*., Vol. 51, No. 2, pp. 1743-1753, Mar. 2015.
[37] D. G. Holmes, T. A. Lipo, B. P. McGrath, and W. Y. Kong, "Optimized design of stationary frame three phase AC current regulators," *IEEE Trans. Power Electron*., Vol. 24, No. 11, pp. 2417-2426, Nov. 2009.

Zhanfeng Song was born in Hebei, China, in 1982. He received the B. S., M. S., and Ph. D. degrees from the Tianjin University, Tianjin, China, in 2004, 2006, and 2009, respectively, all in electrical engineering. He is currently an Associate Professor of Electrical Engineering at the School of Electrical and Information Engineering, Tianjin University, China. His research interests include electrical machines and their control systems. He was the recipient of the 2018 Best Paper Award, First Prize, from IEEE Industry Applications Society Industrial Drives Committee. He served as a Guest Editor for IEEE Transactions on Industrial Informatics.

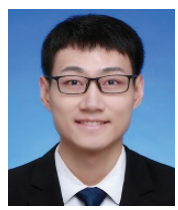

Yun Yu was born in Jiangsu, China, in 1993. He received the B.S. degree in electrical engineering from China University of Mining and Technology, Xuzhou, China, in 2016. He is currently working towards the M.S. degree in electrical engineering, at the School of Electrical and Information Engineering, Tianjin University, China. His research interests include electrical drives and power electronics.

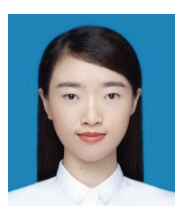

Yaqi Wang was born in Jiangsu, China, in 1995. She received the B.S. degree in automation from Jiangsu University, Zhenjiang, China, in 2017. She is currently working towards the M.S. degree in electrical engineering, at the School of Electrical and Information Engineering, Tianjin University, China. Her research interests include electrical drives and power electronics.

Xiaohui Ma was born in Shanxi, China, in 1996. She received the B.S. degree in Taiyuan University of Technology, Taiyuan, China, in 2018. She is currently working towards the M.S. degree in electrical engineering, at the School of Electrical and Information Engineering, Tianjin University, China. Her research interests include electrical drives and power electronics.